Available online at www.sciencedirect.com

SciVerse ScienceDirect

Ceramics International 38 (2012) 1549–1556

CERAMICS INTERNATIONAL

www.elsevier.com/locate/ceramint

Structural investigation and dielectric studies on Mn substituted $Pb(Zr_{0.65}Ti_{0.35})O_3$ perovskite ceramics

Niranjan Sahu [a], S. Panigrahi [a], Manoranjan Kar [b,*]

[a] Department of Physics, National Institute of Technology, Rourkela 769008, Odisha, India
[b] Department of Physics, Indian Institute of Technology Patna, Patna 800013, Bihar, India

Received 30 January 2011; received in revised form 21 September 2011; accepted 21 September 2011
Available online 28 September 2011

Abstract

Polycrystalline samples of manganese substituted lead zirconium titanate (PZMT) with general formula $Pb(Zr_{0.65-x}Mn_xTi_{0.35})O_3$ ceramics have been synthesised by high temperature solid state reaction technique. X-ray diffraction (XRD) patterns were recorded at room temperature to study the crystal structure employing Rietveld technique. All the patterns could be refined to *R3c* space group with rhombohedral symmetry. Bond lengths and angles have been calculated from refined parameters. Microstructural properties of the materials were analysed by scanning electron microscope (SEM) and compositional analysis were carried out by energy dispersive spectrum (EDS) measurements. All the materials exhibit ferroelectric to paraelectric transition. The Curie temperature (T_c) increases with the Mn concentration. We have observed that dielectric constant decreases and AC conductivity increases with the frequency. The correlation between lattice parameters and T_c for the present samples has been observed.

Keywords: Rietveld; Dielectric; PZT; XRD; Perovskite

1. Introduction

Lead zirconate titanate (PZT) with chemical formulae $Pb(Zr_{1-x}Ti_x)O_3$ is a family of ferroelectric compound which have been studied in detail due to their interesting physical and technological properties [1–3]. However, the structure of PZT is the point of discussion till today. For many years, the crystal structure of PZT was thought to be as indicated by the well known phase diagram published by Jaffe et al. [4]. The morphotropic phase boundary (MPB) region mostly defined in the range $0.4 < x < 0.6$. Most of the research interest has been devoted in this region, because of the extremely high piezoelectric response which has numerous technological applications [5–7]. Depending upon the specific requirement of piezoelectric ceramics, suitable compositions of the PZT system may be chosen [8]. Further, various substituents are added in the PZT system and the properties have been tailored to meet requirements for desired applications [9–11]. However, there are a few reports on substituting transition element either in Zr site or Ti site of the composition Zr/Ti = 65/35 which is beyond the MPB [12,13]. In this composition, several groups have shown the better physical properties which can be transformed for industrial applications [9,10]. In last few years, Mn element has attracted researchers for substitution in Zr site of PZT perovskite due to its comparable ionic radius and magnetic nature which leads to design a new multiferroic material [14–17]. There are a few reports on Mn doped in Zr site of PZT material [18–24]. Hysteretic properties of Mn-doped $Pb(Zr_{0.30}Ti_{0.70})O_3$ thin films has been studied by Zhang and Whatmore [19]. Coercive field increases with the Mn concentration in PZT thin films. Tiwari et al. [20,21] have studied structural and dielectric properties of $Pb(Zr_{0.65-x}Mn_xTi_{0.35})O_3$ ceramics. They have prepared the sample by annealing at 900 °C. The grain sizes of their samples are close to 1 μm. They have observed that, the curie temperature (T_c) increases for $x = 0.05$ and then decreases with the Mn concentration.

The effect of Mn modification on PZT(65/35) ceramics shows the improvement of dielectric constant, Curie temperature and dielectric loss. However, there are inadequate reports on correlation between crystal structure and physical properties on Mn doped PZT materials. Hence, detailed study on crystal structure and electrical properties is required to understand the correlation between them.

* Corresponding author. Tel.: +91 61 22552013; fax: +91 61 22277383.
E-mail address: mano@iitp.ac.in (M. Kar).

0272-8842/$36.00
doi:10.1016/j.ceramint.2011.09.040

In the present study we have doped Mn ions in place of Zr in PZT. The detailed crystal structure has been studied by employing Rietveld analysis. The correlation between crystal structure and dielectric properties has been observed. We have observed that, the T_c and maximum dielectric constant increases with the decrease of lattice parameters and bond lengths. The dielectric constant suggests that, the present material can be a potential element for manufacturing multilayer ceramic capacitors.

2. Experimental technique

Perovskite $Pb(Zr_{0.65-x}Mn_xTi_{0.35})O_3$ (Zr/Ti = 65/35) with $x = 0.00$, 0.05, 0.10 and 0.15 ceramics have been prepared by high temperature solid state reaction technique. Stoichiometric ratio of PbO (Loba Chem., Mumbai), ZrO_2 (Loba Chem., Mumbai), MnO_2 (E. Merck India Ltd.), and TiO_2 (E. Merck India Ltd.) with 99.9% purity was weighed by using a high precision electronic balance. The above materials were mixed thoroughly with the help of agate mortar and pestle. The grinding was carried out under acetone till the acetone evaporates from the mortar. The mixture was ball milled for 8 h and presintered at different temperatures with intermediate grindings. Finally the powder was calcined at 900 °C for 8 h. The fine powders of the above compounds were pressed into cylindrical pellets of 6 mm diameter and 1 mm thickness under a uni-axial pressure of 6 ton using a hydraulic press. Polyvinyl alcohol (PVA) was used as the binder to make pellets. Finally the pellets were sintered at 1100 °C for over 4 h in a alumina crucible and 5% extra lead oxide was added to prevent lead loss at high temperature and then cooled to room temperature at the rate of 2 °C min^{-1}. All the above sintering processes were carried out in air. The bulk densities of the sintered samples were measured by the Archimedes principle using distilled water as medium and found to be 97–98% of the theoretical density. XRD pattern at room temperature for the sample was recorded by using Philips PANalytical X'pert – MPD X-ray diffractometer (XRD) (Model-PW3020). The CuKα radiation was used as X-ray source. The machine was operated at 35 kV and 30 mA in a wide range of Bragg angles 2θ ($20^\circ \leq 2\theta \leq 80^\circ$). The data was collected with step size of 0.020° and time constant of 1 s. The scanning electron micrograph was recorded using JEOL SEM (JEOL T-330) at room temperature. The compositional analysis was carried out by SEM-EDS.

The dielectric (capacitance and dissipation) and impedance parameters were obtained at an input signal level of 1.3 V in a wide temperature range of 40–500 °C and frequency range of 100 Hz–100 kHz using a computer-controlled LCR HiTESTER/Impedance analyser (HIOKI 3522-50). The temperature variation was obtained by a high temperature furnace (Model: DPI-1200).

We have calculated the average crystallite size by using Scherrer's formulae, Williamson–Hall, and Rietveld method. The Scherrer's formulae can be written as [25],

$$S_C = \frac{\kappa\lambda}{\beta\cos\theta} \quad (1)$$

where constant 'k' depends upon the shape of the crystallite size (0.89, assuming the circular grain), β, Full Width at Half Maximum (FWHM) of intensity vs. 2θ profile, λ is wavelength of the CuKα radiation (0.15418 nm) and θ is the Bragg's diffraction angle. The instrumental broadening factor has been taken into account during the FWHM calculation ($\beta = \sqrt{\beta_{obs}^2 - \beta_{ins}^2}$).

According to Williamson–Hall (WH) method [26], the individual contributions to the broadening of reflections can be expressed as

$$\beta\cos\theta = \frac{k\lambda}{S_C} + 4e\sin\theta \quad (2)$$

where $4e\sin\theta$ is the strain effect on the crystallites. It is mostly the correction of Scherrer's formula by taking into account of strain. The 2θ range of 20° to 80° were used to construct a linear plot of $\beta\cos\theta$ versus $\sin\theta$ (figure not shown), from which the average crystallite size and the strain were obtained using Eq. (2).

A complete expression is used in Rietveld method which can be written as [27,28],

$$FWHM^2 = (U + D_{ST}^2)(\tan^2\theta) + V(\tan\theta) + W + \frac{IG}{\cos^2\theta} \quad (3)$$

where U, V and W are the usual peak shape parameters, IG is a measure of the isotropic size effect, D_{ST} coefficient related to strain. IG and D_{ST} can be refined in Rietveld method.

3. Results and discussions

3.1. Structural and morphology

XRD patterns (not shown) of $Pb(Zr_{0.65-x}Mn_xTi_{0.35})O_3$ for $x = 0.00$, 0.05, 0.10 and 0.15 samples annealed at 800 °C reveal that, the samples are in mixed phase. Hence, these samples were annealed at 900 °C and 1100 °C and, XRD patterns for all the samples are shown in Figs. 1 and 2 respectively. We have observed that the samples are almost in single phase form. All the observed peaks could be indexed using *R3c* space group with rhombohedral symmetry except some minor peaks at 26°, 28° and 34°. These small peaks could be due to growth of tetragonal phase of PZT as the parent composition is very close to the MPB region. However, we have not considered those peaks in our analysis as they are very small.

The XRD patterns for all the samples were analysed with the help of Fullprof program by employing Rietveld refinement technique [27,28]. Typical refined XRD pattern of $Pb(Zr_{0.60}Mn_{0.05}Ti_{0.35})O_3$ sample (annealed at 1100°C) is shown in Fig. 3. We have observed that all the peaks could be well refined to *R3c* spacegroup. Lattice parameters, occupancy, fractional atomic positions, etc. were taken as the free parameter during the fitting. The lattice parameters, goodness of the fitting are listed in Table 2. The fractional atomic positions are Pb (0, 0, 0.29030), Zr/Ti (0, 0, 0.01776) and O (0.25963, 0.44976, 0.10665) for $x = 0.00$ (*R3c*) sample. The refined lattice parameters are listed in Table 2. These values are comparable to those of the literature reported values

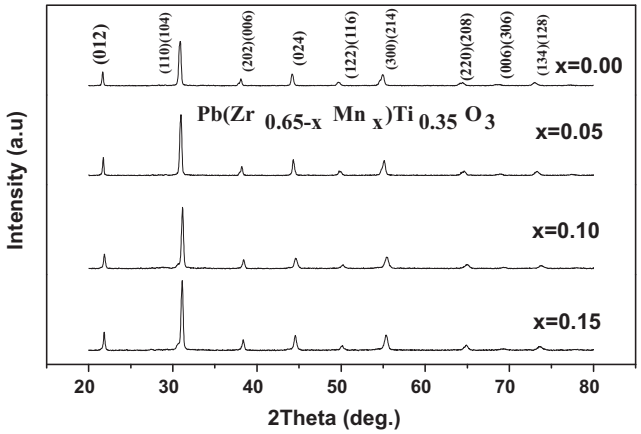

Fig. 1. XRD patterns of the samples $Pb(Zr_{0.65-x}Mn_xTi_{0.35})O_3$ for $x = 0.00$, 0.05, 0.10 and 0.15 (annealed at 900°C for 4 h).

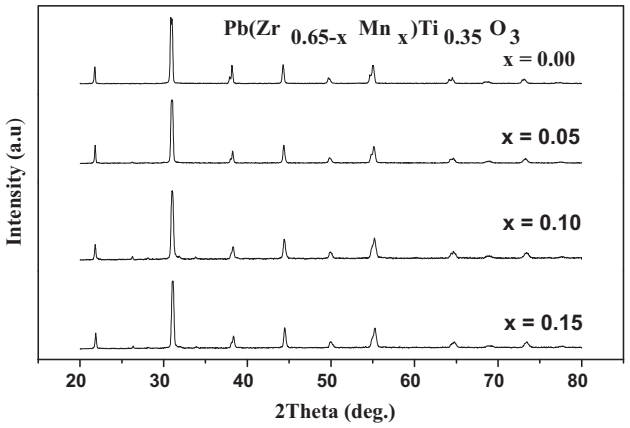

Fig. 2. XRD patterns of the samples $Pb(Zr_{0.65-x}Mn_xTi_{0.35})O_3$ for $x = 0.00$, 0.05, 0.10 and 0.15 (annealed at 1100°C for 4 h).

[29,30]. The lattice parameters and unit cell volume are found to be decreased with the increase of Mn concentration up to $x = 0.10$. It could be due to the smaller ionic size of Mn^{4+} (0.53 Å) to that of ionic size of Zr^{4+} (0.72 Å). Although we have observed decrease of lattice parameters and unit cell volume for $x = 0.15$, but the values are almost comparable to that of $x = 0.10$. It could be due to the segregation of the Mn for $x = 0.15$ sample. However, we have not observed from our XRD pattern. It requires detailed further study by different techniques. Bond angles and lengths were calculated from the refined parameters and typical values are listed in Table 2 for all the samples. It is observed that, the typical bond lengths Pb-Ti/Zr/Mn and Ti/Zr/Mn-O decreases with the Mn concentration up to $x = 0.10$. Although we have observed decrease of bond lengths for $x = 0.15$, but the values are almost comparable to that of $x = 0.10$. The above effects cause the increase of curie temperature (T_c) and ac conductivity with Mn concentration which has discussed in the next section. Bond angles $\angle Pb - Ti/Zr/Mn - Pb$ and $\angle Pb - Ti/Zr/Mn - O$ are almost constant with the Mn concentration.

The average crystallite sizes calculated by using Scherrer's formulae (Eq. (1)), Williamson–Hall (WH) method (Eq. (2)) and Rietveld method (Eq. (3)) are listed in Table 1 for both 900 °C and 1100 °C annealed samples. One can notice that the crystallite size obtained by Rietveld is less than that of WH method. It could be due to the correction of peak broadening taking into account of all instrumental factors. Also particle

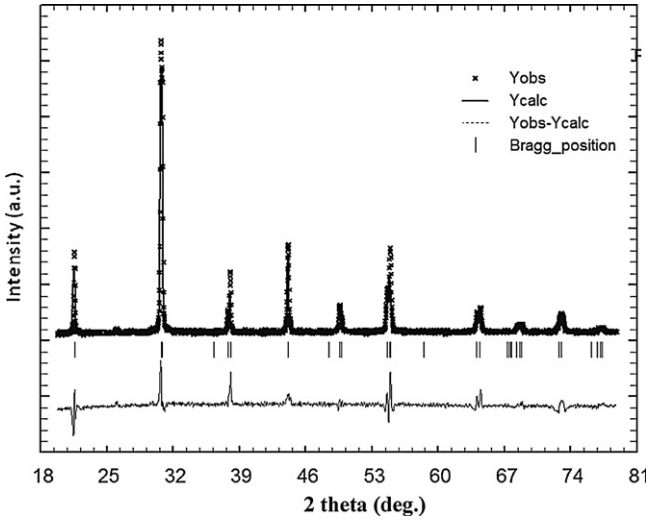

Fig. 3. XRD pattern along with Rietveld refined data for the sample $PbZr_{0.60}Mn_{0.05}$ $Ti_{0.35}O_3$. Sample is annealed at 1100 °C for over 4 h. The patterns has refined using *R3c* space group. The '+' signs represent experimental points and solid line represents Rietveld refined data. The dotted lines show the difference between experimental and refined data.

sizes obtained by WH method are less than those obtained by Scherrer's formulae. It is because, the strain correction factor has been taken into account in case of WH method where as it has not taken into account in Scherrer's method. We have observed that average crystallite size increases with annealing

Table 1
Crystallite size and grain size of the sample $Pb(Zr_{0.65-x}Mn_xTi_{0.35})O_3$ powders for $x = 0$, 0.5, 0.10, and 0.15 annealed at 900 °C for 8 h and 1100 °C for 4 h.

Sample composition	Crystallite size (nm)			Grain size (μm), SEM
	Scherrer method	WH method	Rietveld method	
$Pb(Zr_{0.65}Ti_{0.35})O_3$ (900 °C)	16.8(4)	14.3(3)	13.5(1)	0.114
$Pb(Zr_{0.65}Ti_{0.35})O_3$ (1100 °C)	34.6(4)	33.2(3)	33.0(1)	3.513
$Pb(Zr_{0.60}Mn_{0.05}Ti_{0.35})O_3$ (900 °C)	15.9(4)	13.7(3)	12.8(1)	0.110
$Pb(Zr_{0.60}Mn_{0.05}Ti_{0.35})O_3$ (1100 °C)	32.5(4)	31.9(3)	30.3(1)	3.323
$Pb(Zr_{0.55}Mn_{0.10}Ti_{0.35})O_3$ (900 °C)	15.1(4)	13.0(3)	12.5(1)	0.103
$Pb(Zr_{0.55}Mn_{0.10}Ti_{0.35})O_3$ (1100 °C)	32.0(4)	31.4(3)	30.1(1)	3.313
$Pb(Zr_{0.50}Mn_{0.15}Ti_{0.35})O_3$ (900 °C)	13.7(4)	12.3(3)	11.0(1)	0.101
$Pb(Zr_{0.50}Mn_{0.15}Ti_{0.35})O_3$ (1100 °C)	30.2(4)	28.9(3)	28.0(1)	3.304

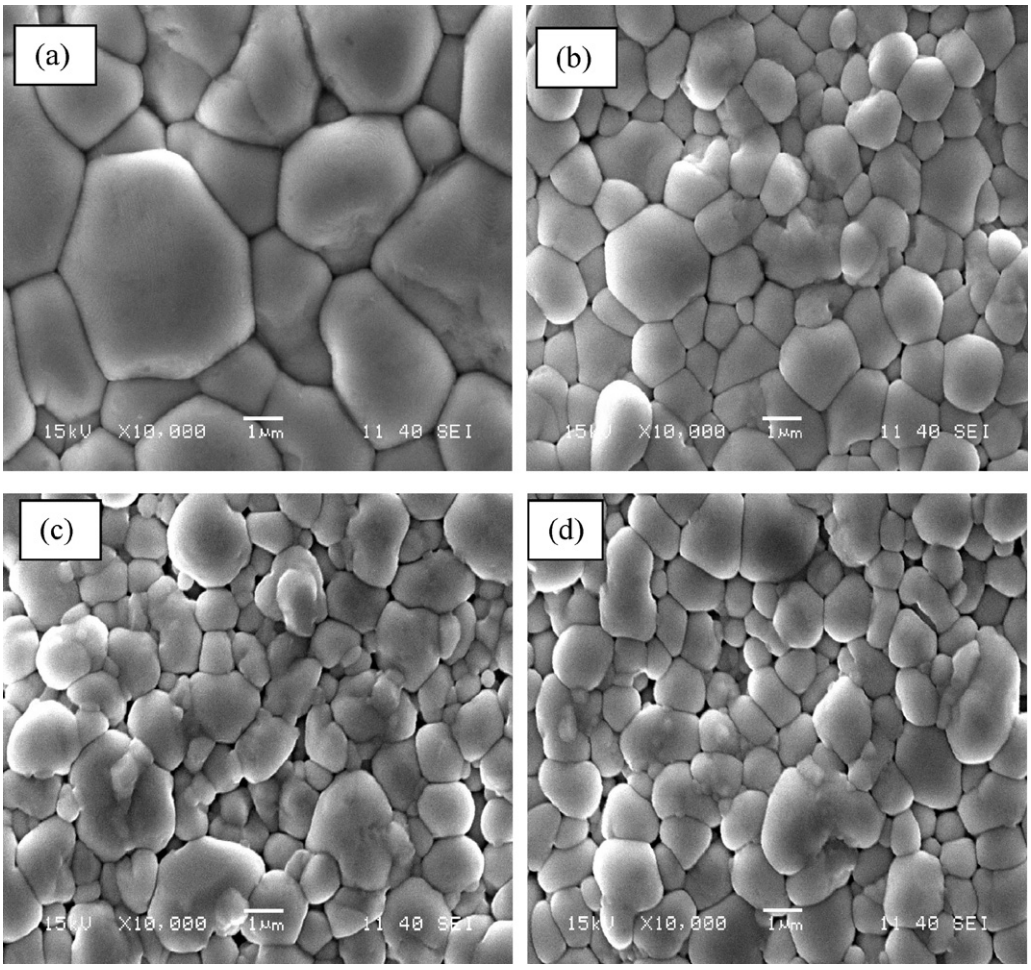

Fig. 4. Micrographs of $Pb(Zr_{0.65-x}Mn_xTi_{0.35})O_3$ for (a) $x = 0.00$, (b) 0.05, (c) 0.10 and (d) 0.15 samples (sintered at 1100 °C for 4 h).

Table 2
Parameters obtained from Rietveld analysis of $Pb(Zr_{0.65-x}Mn_xTi_{0.35})O_3$ powders with ($x = 0$, 0.5, 0.10, and 0.15) annealed at 1100 °C for 4 h.

Sample Parameters	$X = 0.00$	$X = 0.05$	$X = 0.10$	$X = 0.15$
Space group	*R3c*	*R3c*	*R3c*	*R3c*
Pb(Occup.)	0.9863(9)	0.9873(8)	0.9912(7)	0.9885(8)
Zr(Occup.)	0.6423(7)	0.6012(9)	0.5439(9)	0.5043(9)
Mn(Occup.)	–	0.0476(9)	0.0966(8)	0.1489(7)
Ti(Ocuup.)	0.3465(9)	0.3424(9)	0.3482(9)	0.3464(9)
$a = b$(Å)	5.8157(10)	5.7863(12)	5.7797(14)	5.7789(17)
C(Å)	14.1959(34)	14.2746(32)	14.2614(38)	14.2557(49)
Volume (Å^3)	415.08(14)	413.89(15)	412.58(18)	412.31(20)
χ^2 (chi^2)	1.86	2.99	2.68	2.70
R_p	11.9	16.1	15.9	15.5
Rwp	16.3	22.1	21.3	20.9
R_{Bragg}	15.6	15.7	14.7	15.6
R_f	12.8	10.4	10.8	15.3
R_{exp}	11.9	11.5	12.1	12.7
Pb-Ti/Zr/Mn (Å)	3.4667(9)	3.4515(11)	3.4476(12)	3.4471(11)
Ti/Zr/Mn-O (Å)	1.5667(11)/2.6011(13)	1.5663(12)/ 2.5942(12)	1.5651(16)/ 2.5914(12)	1.5647(11)/ 2.5909(14)
∠Pb − Ti/Zr/Mn − Pb	114.12(14)	114.34(11)	114.35(9)	114.35(7)
∠Pb − Ti/Zr/Mn − O	119.02(11)	119.28(7)	119.28(18)	119.29(21)

Table 3
Atomic percentage of the samples $Pb(Zr_{0.65-x}Mn_xTi_{0.35})O_3$ for $x = 0.0$, 0.05, 0.10 and 0.15 (annealed at 1100 °C) obtained from SEM-EDS.

Sample	O wt% (Atomic%)	Zr wt% (Atomic%)	Mn wt% (Atomic%)	Ti wt% (Atomic%)	Pb wt% (Atomic%)
$Pb(Zr_{0.65}Ti_{0.35})O_3$	14.94 (60.38)	18.71 (13.26)	0.00 (0.00)	5.44 (7.35)	60.91 (19.01)
$Pb(Zr_{0.60}Mn_{0.05}Ti_{0.35})O_3$	15.56 (61.79)	17.18 (11.97)	0.21 (0.24)	5.33 (7.07)	61.72 (18.93)
$Pb(Zr_{0.55}Mn_{0.10}Ti_{0.35})O_3$	15.32 (61.25)	15.26 (10.71)	0.58 (0.68)	5.92 (7.92)	62.92 (19.44)
$Pb(Zr_{0.50}Mn_{0.15}Ti_{0.35})O_3$	16.11 (62.49)	14.61 (9.94)	0.95 (1.07)	6.06 (7.85)	62.27 (18.65)

temperature which is due to the formation of larger crystals at high temperature.

The SEM micrographs of the sample annealed at 1100 °C are shown in Fig. 4. One can notice that the grains are in different shapes and sizes. The grains are in order of micron size. The average grain size of the samples are found to be 1–4 μm. Grain size for all the samples are listed in Table 1. The SEM-EDS analysis reveals that, all the compositions present in the samples are as prepared (atomic percentages are listed in Table 3). Generally Pb evaporates during the high temperature annealing. However we have taken special care by annealing the sample initially at low temperature for longer time and also added 5% lead oxide to the parent compound to avoid lead loss during high temperature annealing. Hence there is no significant evaporation of the Pb. Also we have refined the occupancy during the Rietveld analysis. The refined occupancy is given in Table 2.

3.2. Dielectric and conductivity analysis

Dielectric measurement can give information about the electric properties of a material as a function of frequency and temperature. The analysis of dielectric property measures two electrical characteristics of the materials. One is capacitive which related to the insulating nature of the materials and it represents ability to store the charges and, second one is the conductive nature of the materials which gives the information about the electronic charge transport. Through this analysis, the dielectric constant (ε_r) and dielectric loss ($\tan\delta$) of a material can be determined which will explore the technological application. Plots of temperature variation of the dielectric constant (ϵ_r) measured at different frequencies (100 Hz to 100 kHz) of the sample $Pb(Zr_{0.65-x}Mn_xTi_{0.35})O_3$ for $x = 0.05$, 0.10 and 0.15 (annealed at 1100 °C) are shown in Fig. 5(a)–(c) respectively. The dielectric constant of the samples increases gradually with increasing temperature up to a temperature and thereafter it decreases. Dielectric constant increases with temperature due to interfacial polarisation becoming more dominant compared to the dipolar polarisation [31]. After a certain temperature reached, the dielectric constant decreases due to the phase transition from ferroelectric to paraelectric. The transition temperature is called Curie temperature (T_c) which was obtained from $|d\epsilon_r/dT|$ versus temperature plot and those values are given in Table 4. We have observed that, the T_c increases with the Mn concentration up to $x = 0.10$. Although we have observed increase of T_c for $x = 0.15$, but the value is almost comparable to that of $x = 0.10$. It is due to the decrease of lattice parameters, and bond lengths.

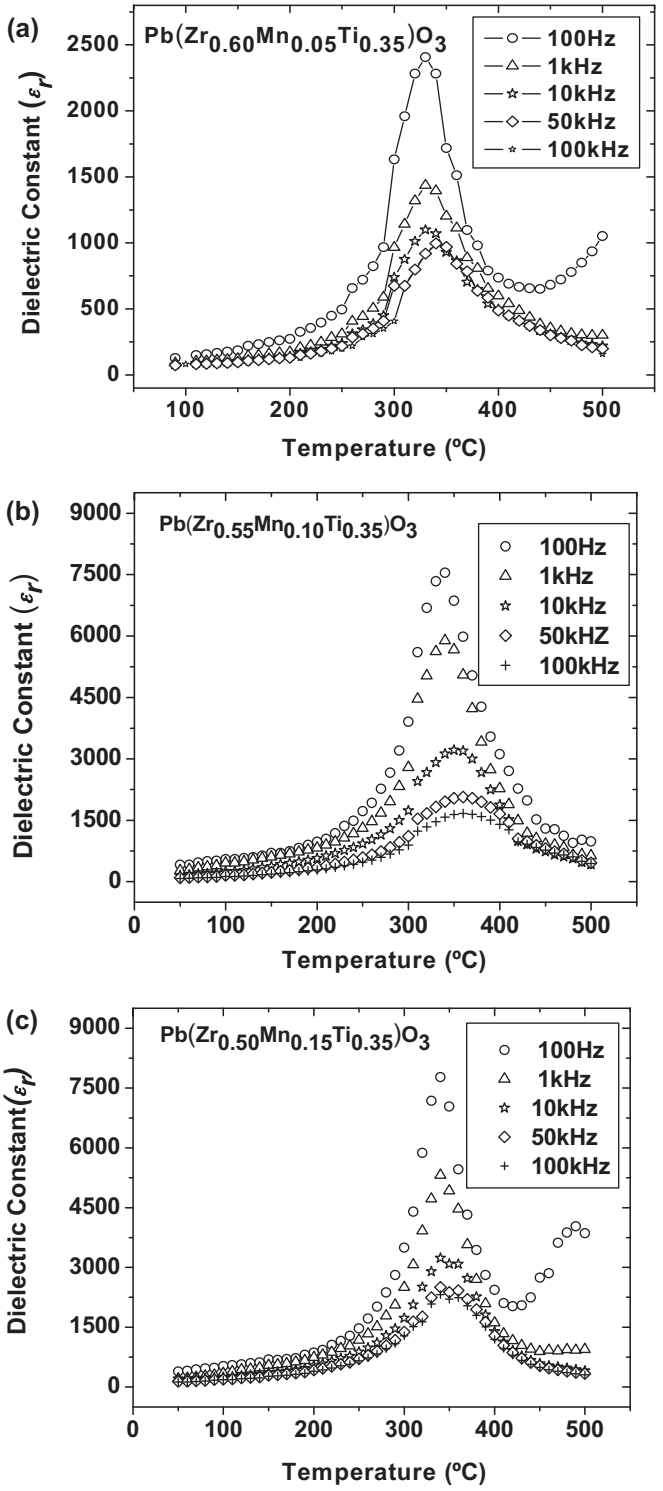

Fig. 5. (a–c) Variation of dielectric constant of $Pb(Zr_{0.65-x}Mn_xTi_{0.35})O_3$ for ($x = 0.05, 0.10, 0.15$) ceramics at different frequencies as a function of temperature.

Table 4
Dielectric data of the sample $Pb(Zr_{0.65-x}Mn_xTi_{0.35})O_3$ for $x = 0.05$, 0.10 and 0.15 at different frequencies.

Compositions	T_c (°C)	ε_r	Frequency (kHz)
$X = 0.05$	329	2405	0.1
	331	1443	1
	332	1097	10
	340	1006	50
	348	934	100
$X = 0.10$	340	7583	0.1
	340	5726	1
	352	3241	10
	355	2055	50
	360	1668	100
$X = 0.15$	341	7791	0.1
	341	5305	1
	349	3241	10
	349	2438	50
	351	2193	100

We have observed a second peak near the temperature ~500 °C only for the measurement at the frequency 100 Hz. The polarisation at low frequencies is due to the contribution of multi component of polarisability such as deformational (electronic and ionic) and relaxation (orientational and interfacial) polarisations (discussed in next section). The space charge polarisation due to impendance charge carriers by interfaces occurs only at low frequencies (1–10^3 Hz). So the second peak at high temperature (only for100 Hz) may be due to space charge polarisation.

Plots of frequency versus dielectric constant for $x = 0.0$, 0.05, 0.10 and 0.15 are shown in Fig. 6(a)–(d) respectively for selected temperatures. It is observed that, the dielectric constant decreases with frequency for all the samples. This can be explained in the fact that, at low frequencies ε_r is due to the contribution of multi component of polarisability, such as deformational (electronic and ionic) and relaxation (orientational and interfacial) polarisations. Electronic polarisation arises from the displacement of the valence electrons relative to the positive nucleus. This type of polarisation takes place up to the frequency 10^{16} Hz. Ionic type of polarisation occurs due to the displacement of negative and positive ions with respect to each other. Maximum frequency of ionic polarisation is 10^{13} Hz. Dipolar polarisation occurs if the materials contain molecules with permanent electric dipole moment that can change orientation into the direction of the applied electric field. The dipolar polarisation takes place at frequencies up to 10^{10} Hz. Space charge polarisation occurs due to impedance mobile charge carriers by interfaces. It occurs at frequency range from 1 to 10^3 Hz. The total polarisation of the dielectric material can be explained as the sum of these 4 types of

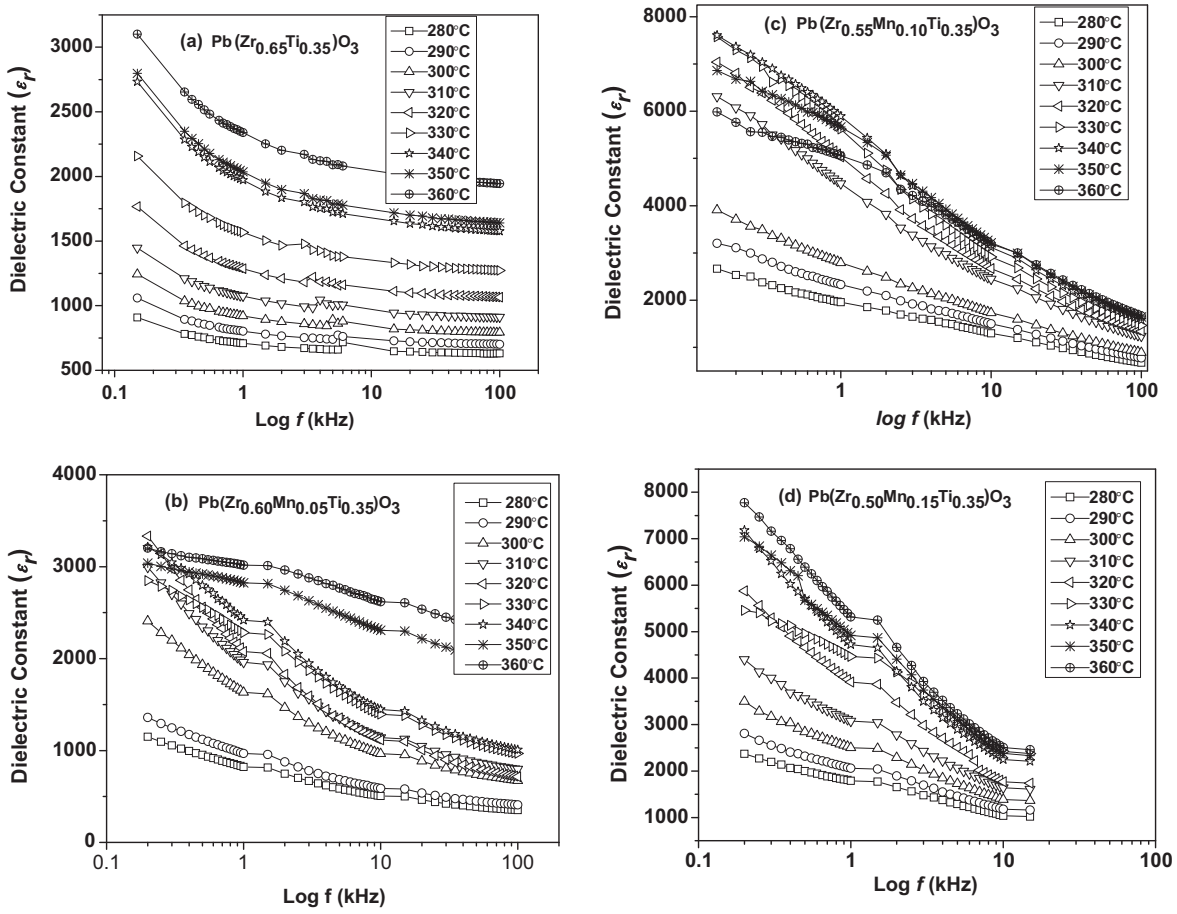

Fig. 6. Variation of dielectric constant (at different temperatures) with the frequency of $Pb(Zr_{0.65-x}Mn_xTi_{0.35})O_3$ samples for (a) $x = 0.00$, (b) $x = 0.05$, (c) $x = 0.10$ and (d) $x = 0.15$. For clarity x-axis has shown in logarithmic scale.

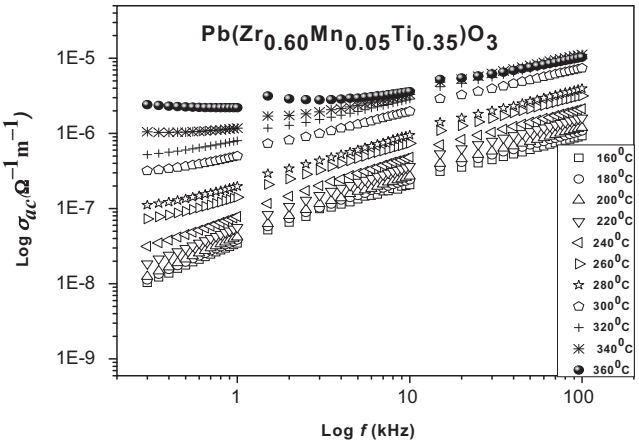

Fig. 7. Variation of ac conductivity with frequency at different temperatures (selected) of $Pb(Zr_{0.60}Mn_{0.05}Ti_{0.35})O_3$ samples. For clarity both *x* and *y* axes are shown in logarithmic scale.

polarisations [15,32]. When the frequency is increased, the orientational polarisation decreases since it takes more time than electronic and ionic polarisations. This decreases the value of relative dielectric constant ε_r reaching a constant value at higher frequency correspondingly to interfacial polarisation. On the other hand the dielectric constant with temperature can be attributed to the fact that the orientational polarisation is connected with thermal motion of molecules so dipole cannot orient themselves at low temperatures. When the temperature is increased the orientation of dipole is facilitated and this increase the orientational polarisation which leads to increase of the dielectric constant with temperature. However after a certain temperature, the thermal energy is very high to restrict the polarisation which leads to the disorder state (paraelectric). Hence, we have observed a transition from ferroelectric to paraelectric phase with the temperature.

The dielectric loss (figure not shown) decreases with frequency and increases with temperature. This is a typical behaviour of ferroelectric materials. Dielectric loss mostly consists of two contributions, such as dielectric polarisation process and DC conduction.

The ac conductivity σ_{ac} of the PZMT ceramic materials at different frequencies and temperatures was calculated using the relation [33],

$$\sigma_{ac} = \omega\varepsilon_o\varepsilon_r \tan\delta \quad (4)$$

Symbols have their usual meanings. Fig. 7 shows the typical variation of ac conductivity of $Pb(Zr_{0.60}Mn_{0.05}Ti_{0.35})O_3$ ceramics as a function of frequency at different temperatures. All the compositions show dispersion of ac conductivity in both the low and high frequency regions. The existence of low frequency dispersion indicates that the charge carriers may be either ionic or electronic nature. The ac conductivity shows an increase with increase in Mn concentration at all frequencies. We have observed that the ac conductivity increase with the decrease of lattice parameters, unit cell volume and bond lengths. It is obvious as, the hoping length for conducting electrons decreases with the decrease of bond lengths.

4. Conclusions

The Mn modified lead zirconate titanate has been prepared in single phase form. The XRD patterns could be refined to *R3c* spacegroup. The lattice parameters and unit cell volumes are found to decrease with the increase of Mn concentration, it could be due to the smaller ionic size of Mn^{4+} (0.53 Å) to that of ionic size of Zr^{4+} (0.72 Å). All the samples exhibit ferroelectric to paraelectric transition. The dielectric constant decreases with the frequency which suggests that the polarisation at low frequency is due to the 4 types of polarisations (deformational (electronic and ionic) and relaxation (orientational and interfacial)). However, the orientational polarisation decreases with frequency since it takes more time than electronic and ionic polarisations. We have observed that dielectric constant (ε_r) is a constant value at higher frequency, which suggests that the present material can be used to manufacturing of multilayer ceramic capacitors. The charge carriers may be either ionic or electronic nature in low frequency region. The ac conductivity increases with the increase in Mn concentration at all frequencies. The increase of T_c and ac conductivity has been observed which may be due to the decrease of lattice parameters, cell volume and bond lengths with the increase of Mn concentration.

Acknowledgements

We are grateful to Dr. A. K. Thakur, Department of Physics and Meteorology, Indian Institute of Technology, Kharagpur 721302, India for his useful suggestions and extend his lab for dielectric measurements.

References

[1] N. Setter, L.E. Cross, The role of B-site cation disorder in diffuse phase transition behavior of perovskite ferroelectrics, J. Appl. Phys. 51 (1980) 4356–4360.
[2] L.E. Cross, Relaxor ferroelectric, Ferroelectrics 76 (1987) 241–267.
[3] J.F. Scott, Ferroelectric Memories, Springer, Berlin, Heidelberg, 2000.
[4] B. Jaffe, W.R. Crook, H. Jaffe, Piezoelectric Ceramics, Academic Press, New York, 1971.
[5] C. Prakash, O.P. Thakur, Pran Kishan, Improvement in material figure of merit of PLZT by samarium substitution, Ferroelectrics 263 (2001) 61–66.
[6] O.P. Thakur, C. Prakash, A.R. James, Enhanced dielectric properties. Ceramics through improved processing, J. Alloys Compd. 470 (2009) 548–551.
[7] P. Novak, J. Kunes, L. Chaput, W.E. Pickett, Exact exchange for correlated electrons, Phys. Stat. Sol. B 243 (2006) 563–572.
[8] H. Yokota, N. Zhang, A.E. Taylor, P.A. Thomas, A.M. Glazer, Crystal structure of the rhombohedral phase of $PbZr_1-xTixO_3$ ceramics at room temperature, Phys. Rev. B 80 (2009) 104109–104121.
[9] S. Singh, O.P. Thakur, D.S. Rawal, C. Prakash, K.K. Raina, Improved properties of Sm substituted PCT ceramics using microwave sintering, Mater. Lett. 59 (2005) 768–772.
[10] G.H. Heartling, Ferroelectric ceramics: history and technology, J. Am. Ceram. Soc. 82 (1999) 797–818.
[11] M.D. Johannes, D.J. Singh, Crystal structure and electric field gradients of $PbZrO_3$ from density functional calculations, Phys. Rev. B 71 (2005) 212101–212104.
[12] A.G. Petukhov, I.I. Mazin, L. Chionel, A.I. Lichtenstein, Correlated metals and the LDA+U method, Phys. Rev. B 67 (2003) 153106.

[13] N. Sahu, M. Kar, S. Panigrahi, Rietveld refinement, microstructure and electrical properties of $PbTiO_3$ ceramic materials, Arch. Phys. Res. 1 (2010) 75–87.
[14] M.P. Moret, M.A.C. Devillers, K. Wörhoff, P.K. Larsen, Optical properties of $PbTiO_3$, $PbZr_xTi_{1-x}O_3$, and $PbZrO_3$ films deposited by metalorganic chemical vapor on $SrTiO_3$, J. Appl. Phys. 92 (2002) 468–474.
[15] D.K. Mahato, R.K. Choudhary, S.C. Srivastava, Dielectric and piezoelectric behaviour of spray dried $Pb_{1-3x/2}$ Smx $(Zr_{0.53}Ti_{0.47})O_3$ ceramic system, J. Appl. Sci. 6 (2006) 716–720.
[16] M.I. Toacsan, A. Ioachim, L. Nedelcu, H.V. Alexandru, Accelerate ageing of PZT-type ceramics, Prog. Solid State Chem. 35 (2007) 531–537.
[17] N. Sahu, M. Kar, S. Panigrahi, Rietveld refinement of a nanocrystalline $Pb_{0.5}Zr_{0.5}TiO_3$ ceramics, Int. J. Phys. 3 (2010) 157–164.
[18] B. Tiwari, R.N.P. Choudhary, Frequency-temperature response of $Pb(Zr_{0.65-x}Ce_xTi_{0.35})O_3$ ferroelectric ceramics: structural and dielectric studies, Physica B 404 (2009) 4111–4116.
[19] Q. Zhang, R.R. Whatmore, Hysteretic properties of Mn-doped $Pb(Zr,Ti)O_3$ thin films, J. Eur. Ceram. Soc. 24 (2004) 277–282.
[20] B. Tiwari, R.N.P. Choudhary, Complex impedance spectroscopic analysis of Mn modified $Pb(Zr_{0.65-x}Mn_xTi_{0.35})O_3$ electroceramics, J. Phys. Chem. Solids 69 (11) (2008) 2852–2857.
[21] B. Tiwari, R.N.P. Choudhary, Effect of Mn-substitution on structural and dielectric properties of $Pb(Zr_{0.65-x}Mn_xTi_{0.35})O_3$ ceramics, Solid State Sci. 11 (2009) 219–223.
[22] S. Sen, P. Pramanik, R.N.P. Choudhary, Effect of Ca-additions on structural and electrical properties of $Pb(SnTi)O_3$ nano-ceramics, Ceram. Int. 33 (2007) 579–587.
[23] S.Y. Kuo, C.-T. Li, W.-F. Hsieh, Decreasing giant splitting of longitudinal and transverse optical phonons in $Pb_xSr_{1-x}TiO_3$ due to Pb covalency, Appl. Phys. Lett. 81 (2002) 3019–3020.
[24] H.B. Park, C.Y. Park, Y.S. Hong, K. Kim, S.J. Kim, Structural dielectric properties of PLZT ceramics modified with lanthanide ions, J. Am. Ceram. Soc. 82 (1999) 94–100.
[25] A. Taylor, X-ray Metallography, Wiley, New York, 1961.
[26] G.K. Williamson, W.H. Hall, X-ray line broadening from field aluminum and wolfram, Acta Met. 1 (1953) 22–31.
[27] R.A. Young, The Rietveld Method International Union of Crystallography, Oxford University Press, New York, 1996.
[28] J. R. Carvajal, FULLPROF 98, A Rietveld Refinement and Pattern Matching Analysis Program, Laboratorie Leon Brillouin (CEA-CNRS), France.
[29] N. Sahu, S. Panigrahi, M. Kar, Structural study of Zr doped $PbTiO_3$ materials by employing Rietveld method, Adv. Powder Tech. (2010).
[30] R. Garg, A. Senyshyn, H. Boysen, R. Ranjan, Structure of the noncubic phase in the ferroelectric state of Pr-substituted $SrTiO_3$, Phys. Rev. B 79 (2009) 144122.
[31] C. Kittel, Introduction to Solid State Physics, John Wiley and Sons Inc., New York/Singapore, 2006.
[32] X.G. Tang, Q.F. Zhou, J.X. Zhang, Raman scattering investigation of the phase transition in nanocrystalline (Pb, Ca, La)TiO_3, J. Appl. Phys. 86 (1999) 5194–5197.
[33] V.M. Gurevich, Electric Conductivity of Ferroelectrics, Moskva, New York, 1969.